European Journal of Radiology 110 (2019) 219–224

Contents lists available at ScienceDirect

European Journal of Radiology

journal homepage: www.elsevier.com/locate/ejrad

Research article

MR textural analysis on contrast enhanced 3D-SPACE images in assessment of consistency of pituitary macroadenoma

Wenting Rui[a,1], Yue Wu[a,1], Zengyi Ma[b], Yongfei Wang[b], Yin Wang[c], Xiao Xu[d], Junhai Zhang[a,*,2], Zhenwei Yao[a,*,2]

[a] Department of Radiology, Huashan Hospital, Fudan University, Mid Wulumuqi Road, Shanghai, 200040, PR China
[b] Department of Neurosurgery, Huashan Hospital, Fudan University, Mid Wulumuqi Road, Shanghai, 200040, PR China
[c] Department of Neuropathology, Huashan Hospital, Fudan University, Mid Wulumuqi Road, Shanghai, 200040, PR China
[d] GE Healthcare Life Sciences, GE Chinese Science and Technology Park, Huatuo Road, Shanghai, 201203, PR China

ARTICLE INFO

Keywords:
Pituitary macroadenoma
Consistency
Textural analysis
3D-SPACE

ABSTRACT

Objectives: To explore the value of magnetic resonance textural analysis (MRTA) in assessing consistency of pituitary macroadenoma (PMA) based on contrast enhanced (CE) three-dimensional sampling perfection with application-optimized contrasts by using different flip angle evolution (3D-SPACE) images.
Materials and methods: Fifty-three patients with PMAs that underwent CE 3D-SPACE scanning by 3.0 T MRI and endoscopic trans-sphenoidal surgery were included in the present study. Consistency levels of PMAs were evaluated intraoperatively by two neurosurgeons. Each resection specimen was stained with H&E and anti-collagen IV. MRTA was conducted and texture features were calculated. An unpaired *t*-test was used to analyze the differences of texture features between soft and hard PMAs. ROC curves by individual and combined features were used to calculate the diagnostic accuracy of MRTA in predicting PMA consistency.
Results: First-order energy and second-order correlation negatively correlated with hard PMAs, while first-order entropy and second-order variance, sum variance, and sum entropy positively correlated with stiffness. All showed significant differences between soft and hard PMAs ($P < 0.05$). Diagnostic accuracy of combined negative features could achieve an AUC of 0.819, sensitivity of 88.9%, specificity of 61.5%, PPV of 70.6%, NPV of 84.2% and positive features could achieve an AUC of 0.836, sensitivity of 85.2%, specificity of 69.2%, PPV of 74.2%, NPV of 81.8% ($P < 0.001$).
Conclusion: MRTA using CE 3D-SPACE images is helpful for assessing PMA consistency preoperatively and noninvasively.

1. Introduction

Pituitary adenoma is the most common intracranial tumor in the sellar region, with an overall prevalence of 16.7% (14.4% in autopsy and 22.5% in radiologic studies) [1]. The incidence of clinically relevant pituitary adenomas is reported in at least 1 in 1064–1289 people [2]. Microadenoma (dimension < 1 cm) and macroadenoma (dimension ≥ 1 cm) account for 57.4% and 42.6%, respectively [3]. Due to obvious hormonal syndromes or neurologic manifestations arising from mass effect, surgical resection is mainly recommended after non-effective medical management, especially for macroadenoma. Endoscopic trans-sphenoidal surgery is the preferred method because of its relative safe nature, especially for adenomas with soft consistency that can easily be curetted by suctioning. Whereas, for macroadenomas with hard consistencies and large suprasellar extensions that need careful separation and resection in a small operation field because of the complex structure of sellar region, craniotomies are more suggested in order to decrease the risk of incomplete resection [4,5]. Preoperative

Abbreviations: PMA, pituitary macroadenoma; MRTA, magnetic resonance textural analysis; 3D-SPACE, three-dimensional sampling perfection with application-optimized contrasts by using different flip angle evolution; CE, contrast enhanced; T2WI, T2-weighted imaging; T1WI, T1-weighted imaging; GLCM, gray level co-occurrence matrix

* Corresponding authors.
E-mail addresses: wennyrui@126.com (W. Rui), wuyue0115@foxmail.com (Y. Wu), zengyima@foxmail.com (Z. Ma), eamns@hotmail.com (Y. Wang), yinwang88@hotmail.com (Y. Wang), adamxu1027@163.com (X. Xu), jhzhang007@fudan.edu.cn (J. Zhang), zwyao@fudan.edu.cn (Z. Yao).
[1] Wenting Rui and Yue Wu contributed equally to this work and share the first authorship.
[2] Zhenwei Yao and Junhai Zhang contributed equally to this work and share the corresponding authorship.

https://doi.org/10.1016/j.ejrad.2018.12.002
Received 22 June 2018; Received in revised form 26 August 2018; Accepted 2 December 2018

evaluation of consistency, especially for macroadenomas, is necessary for determining surgery approach and reducing residuals and recurrence [6].

Previous studies have shown many advantages of contrast enhanced (CE) three-dimensional sampling perfection with application-optimized contrasts by using different flip angle evolution (3D-SPACE) sequences for application in pituitary lesions [7–10]. 3D-SPACE is a turbo spin-echo T2-weighted 3D sequence using variable flip angles for refocusing instead of conventional 180° pulse with less image artifacts and high spatial resolution. Enhanced 3D-SPACE imaging provides both signals of different components on T2-weighted imaging (T2WI) and differential enhancement between the lesion and pituitary. Because of the acquirement of isotropic volumetric data with 0.6 mm slice thickness, the partial volume effect is minimized between imaging of small pituitary lesions and surrounding tissues [8,10]. Besides, due to increased signal intensity of slow flowing fluid filling the cavernous sinus and excellent flow void of internal carotid artery as well as T2 enhanced effect of pituitary adenoma, better contrast of pituitary adenoma with cavernous sinus and clear demonstration of tumor margin for evaluation of cavernous sinus invasion have been verified in previous studies [7,9,11]. In a word, CE 3D-SPACE is superior than routine T2WI and CE T1-weighted imaging (T1WI) for diagnosis of pituitary adenoma, both micro- and macro-adenoma.

Recently, magnetic resonance textural analysis (MRTA) has emerged due to its potential to extract multiple features based on MR images. As an objective strategy, textural analysis provides the quantification of gray-level patterns, pixel inter-relationships, and spectral properties of an image [12]. Namely, global first-order features derived from gray-level intensity histograms, local second-order parameters are calculated on the basis of gray-level co-occurrence matrixes (GLCMs) that reflect the spatial distribution of gray levels and signal intensity interrelationships between adjacent in-plane voxels, and local-regional high-order parameters, such as run-length parameters characterized by run-length matrixes describing the variation in signal intensity level across longitudinal voxels [13]. Previous studies have shown great significance of MRTA in describing tumors' biologic heterogeneity, prediction of therapeutic response, and prognostic biomarkers [14–16]. Therefore, we hypothesized that MRTA based on CE 3D-SPACE images could be applied as a supportive tool in assessing consistency of pituitary macroadenomas (PMAs).

The present study aimed to explore the potential of MRTA using CE 3D-SPACE images for predicting the consistency of PMAs.

2. Materials and methods

2.1. Study population

The study was approved by ethics committee of our institution, and written informed consent for the study was obtained from each patient before participation.

A total of fifty-three patients (mean age: 53 years old; age range: 29–69 years old; 31 males, 22 females) presenting with PMAs (soft: n = 26; hard: n = 27) were recruited for the present study. Participates met the following inclusion criteria: (1) PMA with the diameter over 1 cm; (2) endoscopic trans-sphenoidal surgery performed at our institution with no previous brain operation; (3) CE 3D-SPACE imaging acquired by 3.0 T MR within one month before neurosurgery operation; and (4) histopathologic evaluation. Cases with heterogeneous consistency level of whole tumor by intraoperative observation or with complete cyst or large hematoma in MRI were excluded, because they were difficult to be placed with suitable ROI.

2.2. MR imaging

MR images were acquired with a 3.0 Tesla system (Magnetom Verio, Siemens, Germany) using an 8-channel head coil. Each patient underwent MR scanning in the following order: sagittal, coronal T1-weighted SE imaging; coronal CE T1-weighted SE imaging, coronal CE 3D-T2 SPACE sequence. The parameters of MRI sequences were as follows: T1-SE: TR/ TE 600/15 ms, flip angle 90°, matrix (coronal: 350 × 512; sagittal: 175 × 256), one excitation, field of view 224 × 230, bandwidth 260 Hz/pixel, and slice thickness 2.5 mm with no intersection gap; SPACE: TR/TE 2000/129 ms, flip angle 120°, matrix 316 × 320, two excitations, field of view 180 × 180, bandwidth 289 Hz/pixel, slice thickness 1 mm with no intersection gap. Enhanced imaging was performed immediately after administering a standard dose (0.1 mmol/kg) of gadopentetate dimeglumine (Beilu, Beijing, China).

2.3. Surgery

All patients included in our study underwent endoscopic trans-sphenoidal pituitary adenoma resection by the same neurosurgeon (with over 15-years experience in pituitary surgery). Immediately after surgery, tumor consistency was assessed by two experienced neurosurgeons (one with over 15-years and the other with over 5-years experience in pituitary surgery) according to the surgical notes and video recordings. Consistency of PMA was classified into two levels: soft (tumor that can be easily removed by aspiration or curettage); hard (tumor that cannot be removed by aspiration or curettage but needs piecemeal resection by a microdissector or tumor forceps).

2.4. Pathologic evaluation

One neuropathologist (with over 15-years experience in neuropathology) who was blinded to the surgical results and MR images performed the histology evaluation. After surgery resection, the tumor specimens were fixed in 4% paraformaldehyde and embedded in paraffin, then cut into slices with a microtome. H&E staining and immunohistochemistry were performed routinely. Evaluation of collagen IV was performed using antibodies against collagen IV (1:50, MS-747-S, LabVision, Waltham, MA, USA). In brief, after antigen retrieval, the sliced tissues were blocked in 3% BSA/PBS and then incubated with above antibodies [5]. The stained images were captured with a Leica DFC290 HD color digital camera linked to a Leica DM1000 microscope (Leica, Solms, Germany) at ×400 microscopic magnification.

2.5. MRTA

First, the preoperative CE 3D-SPACE images in a DICOM format were loaded into the software (Omni Kinetics; GE healthcare, China). Two radiologists blinded to the surgical and pathological information drew the ROI of each case with the same consistent criteria guided by an experienced neuroradiologist (with over 25-years experience in neuroradiology). An arbitrary shaped ROI was placed around the area of the mass in a coronal section that had the largest diameter of tumor, avoiding huge cystic areas and hematoma with reference to T1-SE, CE T1WI and CE 3D-T2 SPACE (Figs. 1 and 2). Then first- and second-order texture feature values of each tumor ROI were automatically calculated by Omni Kinetics software. ROI placement of all cases and calculation of texture features were performed twice by each radiologist. Mean values of each feature were later compared to intraoperative evaluation of tumor consistency.

Within each ROI, 27 first-order features, including histogram features, and 32 second and high-order texture features were calculated. First-order and histogram features describes the distribution of voxel signal intensity values. Energy measures the homogeneity of pixel gray levels of an image and entropy is a measure of the randomness of voxel intensity distribution. Texture features are based on different matrixes, including GLCMs (e.g., inertia, variance, correlation, sum variance, difference variance, sum entropy) and run-length matrixes (e.g., short/long run emphasis, high/low grey level run emphasis). Correlation is a

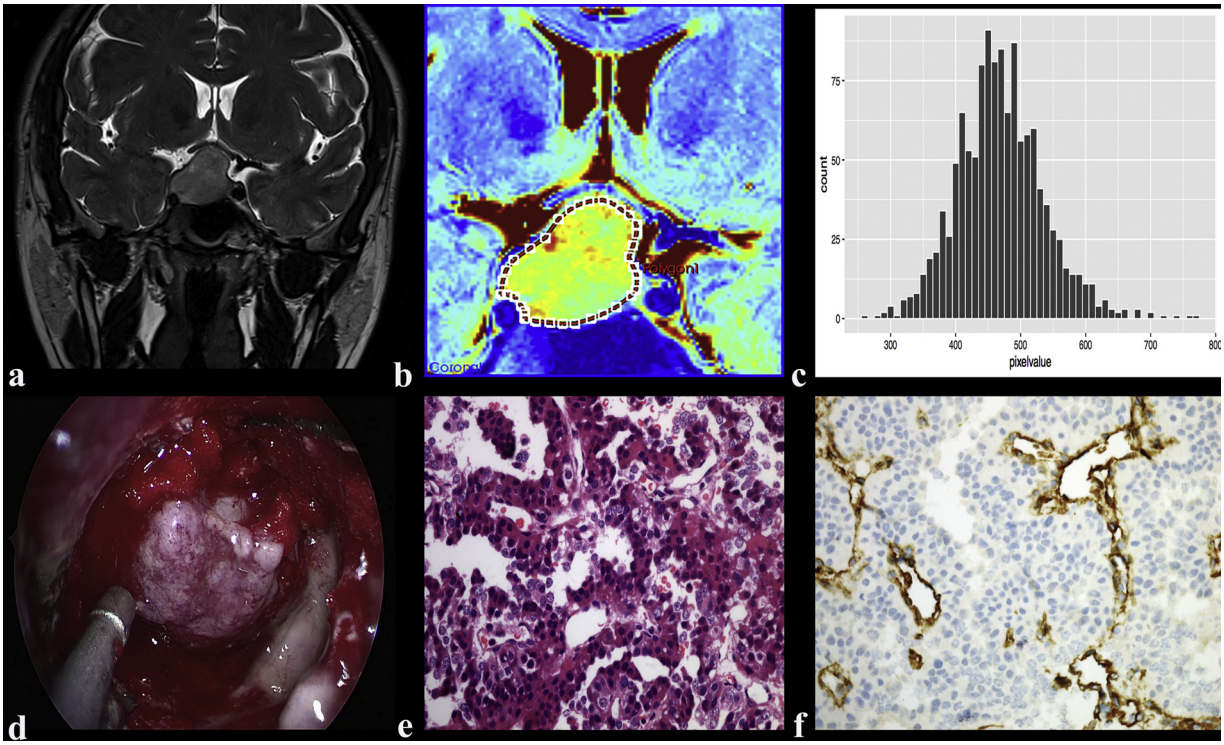

Fig. 1. (a) Coronal CE 3D-SPACE image of a 29-year-old male with non-functional soft PMA; (b) ROI shown on color map of CE 3D-SPACE image; (c) Histogram graph reflecting the distribution of pixel values from the PMA ROI; (d) Surgical finding: soft tumor that can be easily removed by aspiration and curettage; (e) H&E staining of tumor cells showing round small cells (in blue) with scant strip-shaped fibrous stroma (in pink), and high vascularity containing round red blood cells (in pink); (f) Positive anti-collagen IV staining (in brown). 400× microscopic magnification.

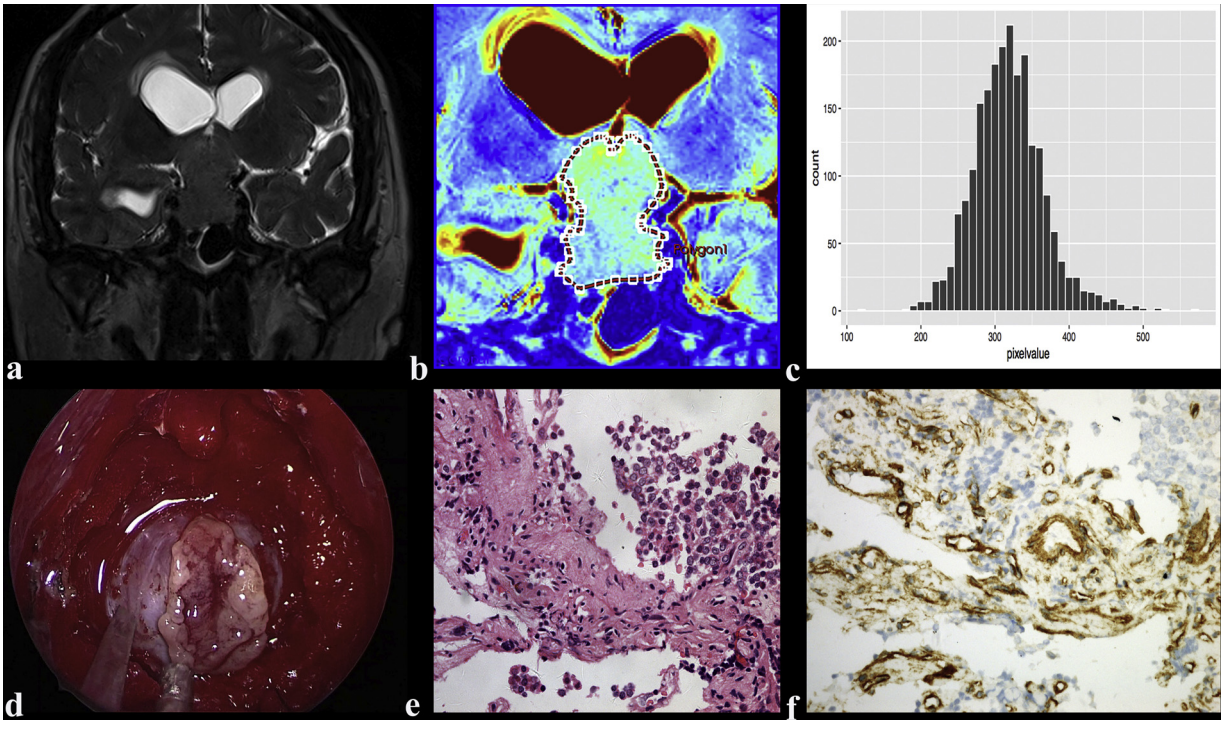

Fig. 2. (a) Coronal CE 3D-SPACE image of a 47-year-old male with non-functional hard PMA; (b) ROI shown on color map of CE 3D-SPACE image; (c) Histogram graph reflecting the distribution of pixel values from the PMA ROI; (d) Surgical finding: hard tumor that cannot be completely removed by aspiration or curettage but needs piecemeal resection by a microdissector; (e) H&E staining of tumor cells showing small cells (in blue) with relatively conspicuous fibrous stroma (in pink); (f) Rich anti-collagen IV staining (in brown). 400× microscopic magnification.

measure of image linearity. High correlation is noted in the image containing a considerable amount of linear structure. Variance measures the dispersion of gray-level differences. Sum variance measures how spread out the sum of the gray levels of voxel pairs is. High sum variance represents greater inhomogeneity. Sum entropy is a measure of the randomness of the sum of the gray level of neighboring pixels.

2.6. Statistical analysis

Agreement of tumor consistency assessment by two neurosurgeons was measured by the kappa test, with kappa values between 0.41-0.60 as moderate, 0.61-0.80 as substantial, and 0.81–1.0 as nearly perfect consistency. Correlation between tumor consistency and content of collagen IV was examined by Spearman's correlation test. Normality tests of MRTA data for each group were analyzed by single-sample Kolmogorov-Smirnov test, which revealed $P > 0.05$ representing normal distribution. Hence, statistical differences of texture features between PMAs with different consistency levels were assessed by the unpaired two-sample *t*-test. Reproducibility and repeatability were assessed by measuring the inter- and intra-observer agreement using intraclass correlation coefficient. The coefficient ≥ 0.75 was interpreted as a good consistency, 0.4-0.75 as fair, and < 0.4 as poor.

ROC curves were performed to assess the diagnostic performance of MRTA, and an optimal threshold value was calculated to quantify the sensitivity and specificity for consistency classification. PPV and NPV were calculated from the ROC analysis. The diagnostic performance was classified as low ($0.5 < AUC \leq 0.7$), moderate to good ($0.7 < AUC \leq 0.9$), and very good to excellent ($0.9 < AUC \leq 1$). Combined ROC analysis was conducted with combined first- and second-order texture features by a binary logistic equation. The best cutoff value was determined according to the Youden index (Youden's J statistic, J = sensitivity + specificity − 1) [17]. All statistical significance was set to 5% and was performed with SPSS v.24 (IBM, Armonk, NY).

3. Results

3.1. Clinical characteristics and correlation with pathological findings

Among the fifty-three PMAs, there were twenty-six ones with soft consistency and twenty-seven ones with hard consistency. The findings were similar between the two assessors (k = 0.90). Expression of collagen IV by anti-collagen staining was positively correlated with the consistency of PMAs (Spearman correlation coefficient = 0.47, $P = 0.002$; Figs. 1 and 2).

We evaluated the fifty-three cases of PMAs included in our study according to endocrine and postoperative immunohistochemistry and observed 30 non-functional PMAs and 23 functional PMAs (two adrenocorticotropic hormone adenomas, two luteinizing hormone adenomas, three growth hormone adenomas, seven follicle-stimulating hormone adenomas, and nine mixed-hormone adenomas).

3.2. Differences of MRTA features between PMAs with different consistency levels

As summarized in Table 1, six features based on MRTA were shown to be statistically significant for assessing the consistency of PMAs. Mathematical formulas and descriptions are listed in Supplemental Online Table 1.

Two first-order parameters, including energy and entropy showed a significant difference (energy: $P = 0.003$; entropy: $P = 0.004$) between soft and hard PMAs. Soft PMAs (n = 26) displayed higher energy (mean ± standard deviation, 0.017 ± 0.005) and lower entropy (6.16 ± 0.49) values compared with hard PMAs (n = 27) (energy: 0.013 ± 0.004, entropy: 6.54 ± 0.43), which reflected increased homogeneous textures in soft PMAs. Histograms of PMAs depicting two consistency levels are shown in Figs. 1 and 2.

Table 1
Statistical analysis of 53 PMAs with soft or hard consistency.

Feature	Texture value (Mean ± SD)		*P*
	Soft	Hard	
First order			
Energy	0.017 ± 0.005	0.013 ± 0.004	0.003
Entropy	6.16 ± 0.49	6.54 ± 0.43	0.004
Second order			
Correlation	0.00067 ± 0.00025	0.00050 ± 0.00015	0.004
Variance	0.067 ± 0.019	0.093 ± 0.028	< 0.001
Sum variance	0.055 ± 0.015	0.079 ± 0.026	< 0.001
Sum entropy	0.86 ± 0.03	0.89 ± 0.02	< 0.001

SD: standard deviation.

Values of second-order feature correlation arising from GLCM were higher in soft PMAs (0.00067 ± 0.00025) compared with hard PMAs (0.00050 ± 0.00015, $P = 0.004$), suggesting more linear structures in relatively soft PMAs. Textures values derived from the Haralick matrix, including variance, sum variance, and sum entropy were all lower in soft PMAs (0.067 ± 0.019, 0.055 ± 0.015, 0.86 ± 0.03, respectively) than in hard PMAs (0.093 ± 0.028, 0.079 ± 0.026, 0.89 ± 0.02, respectively) ($P < 0.001$). These differences implied greater inhomogeneous textures within harder PMAs. No significant difference between run-length matrixes features was found.

3.3. Diagnostic accuracy of MRTA in discriminating consistency levels of PMAs

As summarized in Table 2, first-order features, including energy and entropy, diagnostic performance of which was revealed by AUCs of 0.726 and 0.719, respectively ($P = 0.005$, 0.006, respectively). Second-order texture features based on GLCM and Haralick matrixes exhibited improved diagnostic performances compared with first-order features. CLCM-correlation had an AUC of 0.736, sensitivity of 70.4%, specificity of 76.9%, PPV of 76%, and NPV of 71.4% ($P = 0.003$). Variance, sum variance, and sum entropy based on the Haralick matrix demonstrated AUCs of 0.781, 0.786, and 0.808, respectively ($P < 0.001$). When the Youden index was highest, variance accompanied with the sensitivity of 66.7%, specificity of 80.8%, PPV of 78.3%, and NPV of 70%. Sum variance had the specificity of 100% and PPV of 100%, while sensitivity was 44.4% and NPV was 63.4%. Among all the textures, sum entropy performed best in diagnostic accuracy with an AUC of 0.808, sensitivity of 88.9%, specificity of 65.4%, PPV of 72.7%, and NPV of 85%.

Combined diagnosis by these features negatively correlated with harder consistency, including energy and correlation, achieved with an AUC of 0.819, sensitivity of 88.9%, specificity of 61.5%, PPV of 70.6%, and NPV of 84.2%. Combined ROC analysis of features positively correlated with stiffness, including entropy, Haralick variance, sum

Table 2
ROC analysis of MR textures for assessing consistency levels of PMAs.

Feature	AUC	*P*	YI	COV	S1/S2	PPV	NPV
E1	0.726	0.005	0.359	0.014	66.7/69.2	69.2	66.7
E2	0.719	0.006	0.353	6.13	81.5/53.8	64.7	73.7
C	0.736	0.003	0.473	0.00052	70.4/76.9	76.0	71.4
V	0.781	< 0.001	0.475	0.080	66.7/80.8	78.3	70.0
SV	0.786	< 0.001	0.444	0.083	44.4/100	100	63.4
SE	0.808	< 0.001	0.543	0.87	88.9/65.4	72.7	85.0
E1 + C	0.819	< 0.001	0.504	/	88.9/61.5	70.6	84.2
E2 + V + SV + SE	0.836	< 0.001	0.544	/	85.2/69.2	74.2	81.8

E1: Energy; E2: Entropy; C: Correlation; V: Variance; SV: Sum variance; SE: Sum entropy; YI: Youden Index = sensitivity + specificity − 1; COV: cutoff value; S1(%): sensitivity; S2(%): specificity; "E1 + C" and "E2 + V + SV + SE" represent combined ROC diagnosis based on these features.

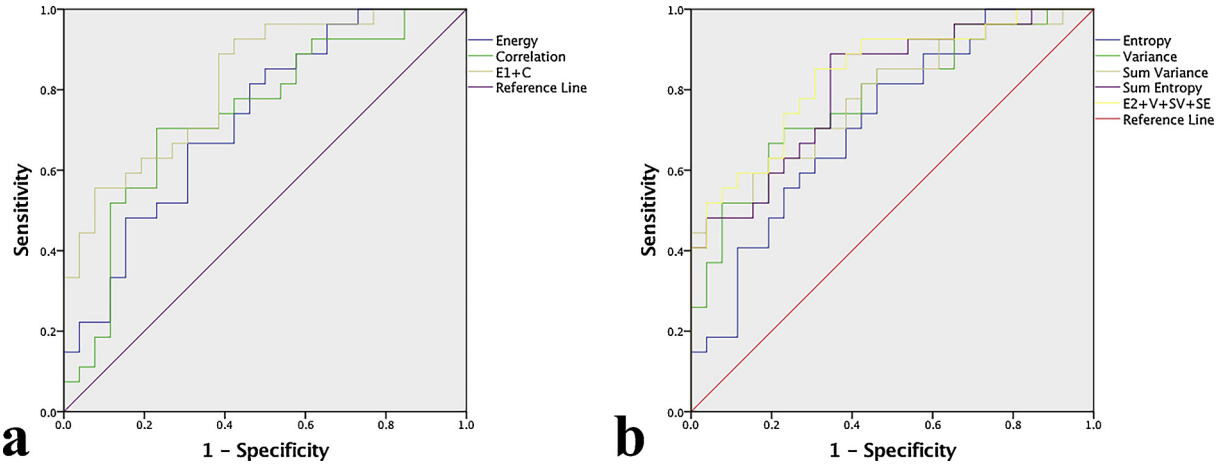

Fig. 3. ROC curves of MRTA features for assessing consistency of PMAs. E1: Energy; E2: Entropy; C: Correlation; V: Variance; SV: Sum variance; SE: Sum entropy. "E1 + C" and "E2 + V + SV + SE" represent combined ROC diagnosis based on these features.

variance, and sum entropy received an AUC of 0.836, sensitivity of 85.2%, specificity of 69.2%, PPV of 74.2%, and NPV of 81.8%. ROC analyses were all statistically significant ($P < 0.001$). All ROC curves are shown in Fig. 3.

3.4. Reproducibility and repeatability measurements

As summarized in Supplemental Online Table 2 and 3, reproducibility and repeatability were measured by inter- and intra-observer correlation coefficient. These coefficients of MRTA features were all higher than 0.80 ($P < 0.05$), reflecting good measurement reliability of MRTA.

4. Discussion

Preoperative knowledge of pituitary adenoma consistency is essential for surgeon to plan appropriate surgery approach. In the present study, we performed MRTA based on CE 3D-SPACE images for predicting the consistency of PMAs preoperatively and quantitatively. First-order and histogram features based on CE 3D-SPACE images, including energy and entropy, were significant in differentiating consistency levels of PMAs. As parameters in measuring homogeneity or heterogeneity of pixel gray levels, a high energy value and low entropy value represented more homogeneous intensity distribution in an image, which was observed in softer PMAs. Second-order texture feature correlation was higher in PMAs with soft consistency, revealing increased linear structures in softer adenomas. Features, including variance, sum variance, and sum entropy based on the Haralick matrix, were higher in PMAs with hard consistency, which represents more inhomogeneous textures in images of hard tumors.

As showed in histograms (Figs. 1 and 2), median of pixelvalue was higher in soft tumors than hard ones, which was consistent with the study based on CE 3D-FIESTA revealing higher signal intensity ratio in soft tumors [18]. However, hard tumors tended to have homogeneous pattern of signal intensity without intratumoral hyperintense dots compared to soft ones on CE 3D-FIESTA images, which seemed to be conflicting with heterogeneous textural features in hard tumors based on CE 3D-SPACE images. An explanation for the imparity may be the differences between the contrast media effect at early or delayed time points on the two sequences. Pathologically, PMAs with soft consistency present with high cellularity that is closely arranged, high vascularization, contain more water and micro-cysts, and less extra-cellar matrix with approximately 7.3% collagen content [19,20]. Whereas, hard PMAs are characterized with scattered moderate-to-low cellularity and low vascularization with abundant extra-cellar matrix containing 17.7% collagenous fiber [19–21]. Due to the sum of the T2 effect and the enhanced effect, signal intensity differences between cells and liquids can be smaller than these between cells and collagen fibers. Hence, an increased content of collagenous fiber augments the inhomogeneity of tumors, which is reflected on CE 3D-SPACE images and detected by MRTA. We postulate that high water content and vascularity may contribute to the increased content of linear structures observed in softer adenomas.

As we know, studies using common MR techniques in evaluating the stiffness of pituitary adenomas showed controversial and inconsistent findings [19,21–23]. A study by Pierallini A et al. demonstrated lower signal intensity ratios of tumor to normal white matter on T2WI and DWI and higher ADC values in hard fibrous tumors [22]. Romano A et al. evaluated twenty-one PMA patients and found signal intensity ratios > 1.92 at early enhanced phase on DCE T1 images were correlated with soft components [21]. However, other studies found no or inverse correlations between tumor consistency and signal intensity ratios on T2WI, CE T1WI, DWI or ADC values [19,23]. Although soft adenomas containing more water may cause increased signal intensity on T2WI, functional pituitary adenomas also secrete proteins that decrease signal intensity on T2WI. DWI has relative lower spatial resolution and artifacts related to bone structure or sinus aeration, application of which in pituitary gland are always controversial. ADC values, which are based on the placement of ROIs, also may be strongly affected. Radiomics approaches including MRTA have shown great advantages in reflecting microscopical texture information contained in images unable to be perceived by human vision. But only a few of such studies concerning pituitary lesions have been reported up to now. To our knowledge, MRTA on CE T1WI was effective for the classification of pituitary tumors, gliomas, and meningiomas [24], and radiomics approach showed potential for the classification of non-functional pituitary adenomas subtypes [25]. In present study, MRTA using high resolution CE 3D-SPACE images achieved good diagnostic accuracy for evaluating the consistency of PMAs (AUCs of 0.819 and 0.836), which corresponded with combined negative and positive first- and second-features that correlated with tumor stiffness. As a noninvasive method, MRTA identifies image heterogeneity preoperatively and may help assess consistency of PMAs, which can guide the appropriate surgery approach to increase resection rates and reduce the long-term risk of recurrence.

Our study has several limitations. First, as consistency of the entire PMA was sometimes inconsistent, the arbitrarily shaped 2D-ROI rather than volume ROI may not have matched pathological slices well. Nevertheless, we selected the PMAs with relative homogeneous consistency to avoid sampling error. Second, non-enhanced 3D-SPACE and

common T2WI with and without MRTA were not performed, which may be compared with present results and better explain the heterogeneity of images. Third, our study had a relative small sample size; a further prospective study, with a larger sample population including test data set and using volume ROI to analyze texture on multi-model MRI will be performed next.

In conclusion, MRTA based on CE 3D-SPACE images shows good diagnostic performance for distinguishing consistency levels of PMAs and will be an important supportive tool for assessing PMA consistency preoperatively and noninvasively.

Conflict of interest

We declare that we have no conflict of interest.

Funding

This research did not receive any specific grant from funding agencies in the public, commercial, or not-for-profit sectors.

Appendix A. Supplementary data

Supplementary material related to this article can be found, in the online version, at doi:https://doi.org/10.1016/j.ejrad.2018.12.002.

References

[1] S. Ezzat, S.L. Asa, W.T. Couldwell, C.E. Barr, W.E. Dodge, M.L. Vance, I.E. McCutcheon, The prevalence of pituitary adenomas: a systematic review, Cancer 101 (2004) 613–619.
[2] A. Beckers, Higher prevalence of clinically relevant pituitary adenomas confirmed, Clin. Endocrinol. 72 (2010) 290–291.
[3] A.F. Daly, M. Rixhon, C. Adam, A. Dempegioti, M.A. Tichomirowa, A. Beckers, High prevalence of pituitary adenomas: a cross-sectional study in the province of Liege, Belgium, J. Clin. Endocrinol. Metab. 91 (2006) 4769–4775.
[4] N. Hoang, D.K. Tran, R. Herde, G.C. Couldwell, A.G. Osborn, W.T. Couldwell, Pituitary macroadenomas with oculomotor cistern extension and tracking: implications for surgical management, J. Neurosurg. 125 (2016) 315–322.
[5] Z. Ma, W. He, Y. Zhao, J. Yuan, Q. Zhang, Y. Wu, H. Chen, Z. Yao, S. Li, Y. Wang, Predictive value of PWI for blood supply and T1-spin echo MRI for consistency of pituitary adenoma, Neuroradiology 58 (2016) 51–57.
[6] M. Losa, P. Mortini, R. Barzaghi, P. Ribotto, M.R. Terreni, S.B. Marzoli, S. Pieralli, M. Giovanelli, Early results of surgery in patients with nonfunctioning pituitary adenoma and analysis of the risk of tumor recurrence, J. Neurosurg. 108 (2008) 525–532.
[7] Y. Wu, J. Wang, Z. Yao, Z. Yang, Z. Ma, Y. Wang, Effective performance of contrast enhanced SPACE imaging in clearly depicting the margin of pituitary adenoma, Pituitary 18 (2015) 480–486.
[8] J. Wang, Y. Wu, Z. Yao, Z. Yang, Assessment of pituitary micro-lesions using 3D sampling perfection with application-optimized contrasts using different flip-angle evolutions, Neuroradiology 56 (2014) 1047–1053.
[9] T. Tong, W. Yue, Y. Zhong, Y. Zhenwei, H. Yong, F. Xiaoyuan, Comparison of contrast-enhanced SPACE and CISS in evaluating cavernous sinus invasion by pituitary macroadenomas on 3-T magnetic resonance, J. Comput. Assist. Tomogr. 39 (2015) 222–227.
[10] Y. Tang, Y. Wu, H. Zhang, J. Wang, Z. Yao, Increased diagnostic confidence in the diagnosis of pituitary micro-lesions with the addition of three-dimensional sampling perfection with application-optimized contrasts using different flip-angle evolutions sequences, Acta Radiol. (Stockholm, Swed. : 1987) (January) (2018), https://doi.org/10.1177/0284185118774954 [Epub ahead of print].
[11] B. Baumert, K. Wortler, D. Steffinger, G.P. Schmidt, M.F. Reiser, A. Baur-Melnyk, Assessment of the internal craniocervical ligaments with a new magnetic resonance imaging sequence: three-dimensional turbo spin echo with variable flip-angle distribution (SPACE), Magn. Reson. Imaging 27 (2009) 954–960.
[12] A. Kassner, R.E. Thornhill, Texture analysis: a review of neurologic MR imaging applications, AJNR. Am. J. Neuroradiol. 31 (2010) 809–816.
[13] S. Gourtsoyianni, G. Doumou, D. Prezzi, B. Taylor, J.J. Stirling, N.J. Taylor, M. Siddique, G.J.R. Cook, R. Glynne-Jones, V. Goh, Primary rectal cancer: repeatability of global and local-regional MR imaging texture features, Radiology 284 (2017) 552–561.
[14] P. Kickingereder, S. Burth, A. Wick, M. Gotz, O. Eidel, H.P. Schlemmer, K.H. Maier-Hein, W. Wick, M. Bendszus, A. Radbruch, D. Bonekamp, Radiomic profiling of glioblastoma: identifying an imaging predictor of patient survival with improved performance over established clinical and radiologic risk models, Radiology 280 (2016) 880–889.
[15] W. Rui, Y. Ren, Y. Wang, X. Gao, X. Xu, Z. Yao, MR textural analysis on T2 FLAIR images for the prediction of true oligodendroglioma by the 2016 WHO genetic classification, J. Magnetic Resonance Imaging: JMRI 48 (November) (2018) 74–83, https://doi.org/10.1002/jmri.25896 < / > .
[16] A. Wibmer, H. Hricak, T. Gondo, K. Matsumoto, H. Veeraraghavan, D. Fehr, J. Zheng, D. Goldman, C. Moskowitz, S.W. Fine, V.E. Reuter, J. Eastham, E. Sala, H.A. Vargas, Haralick texture analysis of prostate MRI: utility for differentiating non-cancerous prostate from prostate cancer and differentiating prostate cancers with different Gleason scores, Eur. Radiol. 25 (2015) 2840–2850.
[17] W.J. Youden, Index for rating diagnostic tests, Cancer 3 (1950) 32–35.
[18] J. Yamamoto, S. Kakeda, S. Shimajiri, M. Takahashi, K. Watanabe, Y. Kai, J. Moriya, Y. Korogi, S. Nishizawa, Tumor consistency of pituitary macroadenomas: predictive analysis on the basis of imaging features with contrast-enhanced 3D FIESTA at 3T, AJNR. Am. J. Neuroradiol. 35 (2014) 297–303.
[19] L. Yiping, X. Ji, G. Daoying, Y. Bo, Prediction of the consistency of pituitary adenoma: A comparative study on diffusion-weighted imaging and pathological results, J. Neuroradiol. 43 (2016) 186–194.
[20] L. Wei, S.A. Lin, K. Fan, D. Xiao, J. Hong, S. Wang, Relationship between pituitary adenoma texture and collagen content revealed by comparative study of MRI and pathology analysis, Int. J. Clin. Exp. Med. 8 (2015) 12898–12905.
[21] A. Romano, V. Coppola, M. Lombardi, L. Lavorato, D. Di Stefano, E. Caroli, M.C. Rossi Espagnet, F. Tavanti, G. Minniti, G. Trillo, A. Bozzao, Predictive role of dynamic contrast enhanced T1-weighted MR sequences in pre-surgical evaluation of macroadenomas consistency, Pituitary 20 (2017) 201–209.
[22] A. Pierallini, F. Caramia, C. Falcone, E. Tinelli, A. Paonessa, A.B. Ciddio, M. Fiorelli, F. Bianco, S. Natalizi, L. Ferrante, L. Bozzao, Pituitary macroadenomas: preoperative evaluation of consistency with diffusion-weighted MR imaging–initial experience, Radiology 239 (2006) 223–231.
[23] O.M. Mahmoud, A. Tominaga, V.J. Amatya, M. Ohtaki, K. Sugiyama, T. Sakoguchi, Y. Kinoshita, Y. Takeshima, N. Abe, Y. Akiyama, A.I. El-Ghoriany, A.K. Abd Alla, M.A. El-Sharkawy, K. Arita, K. Kurisu, F. Yamasaki, Role of PROPELLER diffusion-weighted imaging and apparent diffusion coefficient in the evaluation of pituitary adenomas, Eur. J. Radiol. 80 (2011) 412–417.
[24] J. Cheng, W. Huang, S. Cao, R. Yang, W. Yang, Z. Yun, Z. Wang, Q. Feng, Enhanced performance of brain tumor classification via tumor region augmentation and partition, PloS One 10 (2015) e0140381.
[25] S. Zhang, G. Song, Y. Zang, J. Jia, C. Wang, C. Li, J. Tian, D. Dong, Y. Zhang, Non-invasive radiomics approach potentially predicts non-functioning pituitary adenomas subtypes before surgery, Eur. Radiol. 28 (March) (2018) 3692–3701, https://doi.org/10.1007/s00330-017-5180-6.